Biochemistry

 Volume 31, Number 18 May 12, 1992

Articles

A Comparative Investigation of Snake Venom Neurotoxins and Their Triplet-State Tryptophan–Disulfide Interactions Using Phosphorescence and Optically Detected Magnetic Resonance†

Bruce D. Schlyer,‡ Edmond Lau, and August H. Maki*
Department of Chemistry, University of California, Davis, California 95616
Received November 6, 1991; Revised Manuscript Received February 21, 1992

ABSTRACT: We have investigated the luminescence and optically detected magnetic resonance (ODMR) of the highly homologous snake venom neurotoxins α-bungarotoxin (BgTX), α-cobratoxin (CbTX), and cobrotoxin (CoTX) in frozen aqueous glasses. The phosphorescence intensity and lifetime of the single invariant tryptophan, Trp29, are found to be diminished in BgTX and CbTx relative to CoTX both at 77 K and at 4.2 K. Selective reduction of the Cys30–Cys34 disulfide proximal to Trp29 in BgTX and CbTX, that is absent in CoTX, results in the enhancement of the phoosphorescence to fluorescence intensity ratio of Trp29 and identifies this disulfide as the source of the triplet-state quenching. Variations of the phosphorescence parameters are observed for differently frozen BgTX and CbTX samples. We argue that this observation is consistent with conformational flexibility in the region of Trp29. For BgTX and CbTX, changing the wavelength of excitation from 285 to 300 nm results in a small bathochromic phosphorescence shift of 0.4 nm, an average decrease in the lifetime, and a change in the polarity of the normally positive D–E ODMR signal. From the small excitation-dependent emission shift, we infer that Trp29 is in a relatively hydrophobic environment. The excitation-dependent changes in lifetime and ODMR signal parameters arise from subtle heterogeneity in the disposition of Trp29 with respect to Cys30–Cys34. We discuss the mechanism of disulfide-induced quenching of the Trp29 triplet state in BgTX and CbTX and argue that it most probably is due to electron transfer.

Snake venom neurotoxins bind specifically and tightly to nicotinic acetylcholine receptors (AChR)[1] of postsynaptic membranes, thus producing a neuromuscular block. There are over 60 highly homologous neurotoxins of known primary sequence (Dufton & Hilder, 1983) which are conveniently grouped into 2 classes, short-chain neurotoxins containing 60–62 amino acid residues and long-chain neurotoxins of 70–74 residues.

Numerous studies of the specific effects of chemical modification on acetylcholine receptor binding affinity have been performed on neurotoxins. It is now believed that no one single residue is necessary for binding but that interaction with substrate involves many active areas on the toxin "surface" (Low, 1979). On the basis of sequence homology and modification studies, several residues have been suggested to play a functional role in AChR recognition including the residues Lys27, Trp29, Asp31, Arg37, and Lys53/Arg53 (Low, 1979). Although several numbering schemes have been used to identify specific residues among the homologous neurotoxins, we adopt here the convention of Karlsson (1979) which corresponds to maximal alignment for both short- and long-series neurotoxins. The short-chain neurotoxins contain four disulfide bonds and the long-chain toxins, five. Within both classes of

† This work was supported in part by a National Institutes of Health grant (ES-02662).
* To whom correspondence should be addressed.
‡ Present address: Institute of Gerontology, The University of Michigan, 300 North Ingalls, Ann Arbor, MI 48109.

[1] Abbreviations: AChR, acetylcholine receptor; BgTX, α-bungarotoxin; $BgTX_{red}$, BgTX in which Cys30 and Cys34 are in reduced form; CbTX, α-cobratoxin; $CbTX_{red}$, CbTX in which Cys30 and Cys34 are in reduced form; CoTX, cobrotoxin; DDT, dithiothreitol; HAE, heavy-atom effect; HEWL, hen egg white lysozyme; ODMR, optically detected magnetic resonance.

0006-2960/92/0431-4375$03.00/0

toxins, the four invariant disulfides define a globular crown from which three, roughly parallel, polypeptide loops project. Two of these loops, including the central loop, are involved in a triple-stranded antiparallel pleated β-sheet structure. The overall shape of the molecule is disklike, with the protruding loops forming a cup-shaped surface. In the long-chain neurotoxins, the fifth cystine is found at the end of the long central tail and pinches off this loop into a small, "extra", cyclical polypeptide loop. The extra disulfide of the long-chain forms, Cys30–Cys34, may be selectively reduced with little loss of binding affinity (Botes, 1974; Chicheporte et al., 1975; Martin et al., 1983), suggesting its structural rather than functional role.

Three neurotoxins are of interest to us. Two long-chain toxins, α-bungarotoxin (BgTX), consisting of 74 residues, and α-cobratoxin (CbTX), with 71 residues, both contain the fifth disulfide. The third toxin is the short-chain cobrotoxin (CoTX), containing only 62 residues, and missing the fifth disulfide. The X-ray crystal structure of CbTX has been determined (Walkinshaw et al., 1980) and found to be in general agreement with solution structure studies by NMR and by circular dichroism (Hilder et al., 1982). For the long-chain neurotoxin BgTX, the situation is different. The X-ray crystallographic structure of BgTX (Love & Stoud, 1986) shows significant differences in the location of Trp29 from that determined in solution by several methods (Basus et al., 1988; Inagaki et al., 1985). The latter determinations place Trp29 on the reactive, concave side of the protein, along with Lys27, Asp31, Tyr25, and Arg37, while the crystal structure has Trp29 positioned on the convex, solution-exposed side of the β-pleated structure. The crystal structures of the short-chain neurotoxins erabutoxin a (Corfield et al., 1989) and erabutoxin b (Tsernoglou & Petsko, 1976) have Trp29 placed on the concave side of the β-pleated structure, similar to the solution structure of BgTX and both the crystalline and the solution structure of CbTX. The differences between BgTX crystal and solution structures have been rationalized in terms of the presence of several low-energy conformations with small interconversion barriers. Crystal packing forces are believed to be sufficient to select a minor conformer which is observed in the X-ray experiments (Love & Stroud, 1986; Basus et al., 1988).

The purpose of the present study is 2-fold. First we wish to characterize the Trp29 triplet state of BgTX using phosphorescence and ODMR in preparation for binding studies to synthetic peptides which constitute the major binding determinant of the AChR. It has been suggested that Trp187 of the receptor's α-subunit is important in BgTX binding (Wilson & Lentz, 1988) and also that Trp29 or Tyr25 of BgTX interacts with a receptor tryptophan (Low & Corfield, 1986, 1987). In addition, we are interested in the study of tryptophan triplet states interacting with disulfides. Surveys of protein crystallographic data have shown that there is a greater than random chance for tryptophan to be found in proximity to disulfides and that the interaction geometry places the sulfur atoms along the edge of the indole plane (Reid et al., 1985). Although the number of protein residues that are known to internally quench Trp singlet states is large (Steiner & Kirby, 1969), the direct deactivation of Trp triplet states in frozen media apparently is limited to disulfides (King & Miller, 1976). The effect of disulfides on Trp phosphorescence has been shown recently to be short range in nature (Li et al., 1989) and to proceed via a one- or two-electron-transfer process. Given the high probability for the occurrence of Trp–disulfide encounters, the absence of other internal protein perturbers, and the increased interest in protein phosphorescence as a tool in the study of biomolecules, a clearer picture of Trp–disulfide interactions in the triplet state is called for.

In this study, we present our results using low-temperature phosphorescence emission and ODMR spectroscopies to characterize the triplet state of Trp29 in the long-chain toxins BgTX and CbTX and in the short-chain toxin CoTX. The observation of short-decay components in the triplet-state deactivation of BgTX and CbTX and the small ratio of phosphorescence to fluorescence intensity (Φ_p/Φ_f) suggest the important role of the neighboring Cys30–Cys34 in the triplet-state quenching of Trp29. This is confirmed by the selective reduction of the contiguous cystine which leads to an increase in triplet lifetime and in Φ_p/Φ_f. The absence of a short-lifetime component coupled with the observation of a monoexponential triplet-state lifetime of 6.7 s originating from Trp29 in the short-chain toxin CoTX adds further confidence to the assignment of Cys30–Cys34 as the triplet-state quencher. In both BgTX and CbTX, changes in emission spectra and lifetimes are observed for differently frozen samples. We suggest that these results arise from flexibility in the region of Trp29 in solution creating an array of Trp–disulfide distances and subsequent trapping of slightly different conformations in the frozen glass matrices used in our spectroscopic techniques. Triplet-state properties are found to change with the wavelength of excitation, suggesting heterogeneity in the environment of Trp29. This dependence is most apparent in the ODMR spectra of BgTX and CbTX where changing the excitation wavelenth from 285 to 300 nm results in a reversal in the polarity of the normally positive D–E signal. Subtle differences in Trp–disulfide distances with concomitant changes in triplet-state quencher deactivation rates are postulated to be a contributing factor to the dramatic excitation-dependent ODMR spectra. Finally, we discuss our results and those of others with regard to possible mechanisms of the Trp–disulfide triplet-state interaction. The disulfide-induced Trp29 quenching either may be nonspecific with respect to a particular spin sublevel or may selectively depopulate the spin sublevel which is quantized with respect to the z (out-of-plane) zero-field axis.

Materials and Methods

Samples of BgTX from the Formosan banded krait (*Bungarus multicinctus*) and CbTX from Thailand cobra (*Naja naja siamensis*) were obtained as lyophilized powders from Sigma Chemical Co. and the Miami Serpentarium. Additional BgTX was a generous gift from Mark McNamee of the Department of Biochemistry and Biophysics, University of California, Davis. CoTX, from the venom of the Taiwan cobra (*Naja naja atra*), was purchased from Calbiochem Corp. Hen egg white lysozyme (HEWL) and somatostatin were purchased from Sigma Chemical Co. while L-tryptophan and 3-methylindole were from Aldrich. Toxin protein concentrations were determined spectrophotometrically using molar extinction coefficients at 280 nm of 9.3×10^3 M^{-1} cm^{-1} for BgTX (Kabat & Meyer, 1961), 7.6×10^3 M^{-1} cm^{-1} for CbTX (Martin et al., 1983), and 9.4×10^3 M^{-1} cm^{-1} for CoTX (Chen et al., 1977). The lyophilized toxin samples were reconstituted in water, and their lyophilization buffers were exchanged with water by ultracentrifugation. All of the results reported here pertain to proteins dissolved in water. For low-temperature measurements, 30% ethylene glycol (Fluka Chemie AG) was added to yield protein concentrations between 0.1 and 0.8 mM. The pHs of the samples in cryosolvent and water were measured by the use of a microelectrode (Microelectrodes, Inc.) and adjusted to a value of pH 7 by the addition of HCl or

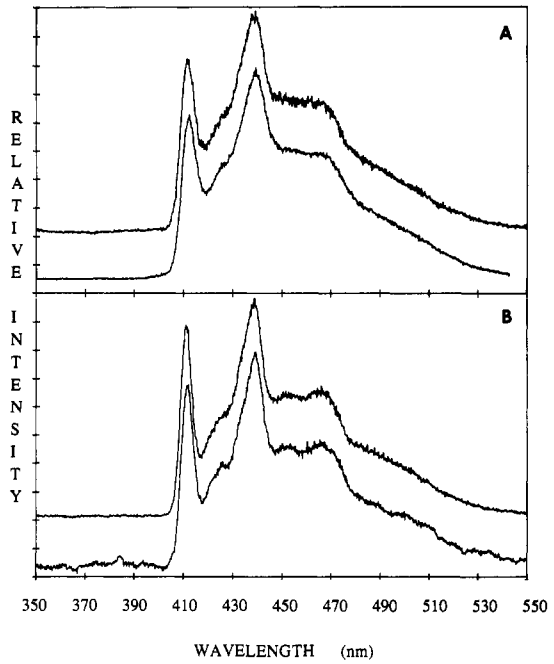

FIGURE 1: Phosphorescence spectra of (A) BgTX and of (B) CoTX observed at 4.2 K. Within each panel, the top spectrum was obtained with excitation centered at 285 nm with 16-nm band-pass and the bottom spectrum with excitation centered at 300 nm with 16-nm bandpass.

NaOH. Selective reduction of the fifth disulfide bond of BgTX and CbTX was accomplished by allowing a 1:1 mixture of protein and freshly prepared dithiothreitol (DDT) to equilibrate at 30 °C for 20 min following the procedure of Martin et al. (1983). The reduced toxins will hereafter be referred to as $BgTX_{red}$ and $CbTX_{red}$. Spectroscopic measurements were made on freshly reduced samples.

The experimental setup and methods used in our laboratory have been described previously (Ghosh et al., 1986). The tryptophan triplet state was photoexcited using a 100-W high-pressure mercury arc lamp filtered by a 11-cm solution of 500 g/L $NiSO_4$ and a 10-cm Jovin-Yvon H10 monochromator (1200 g/mm) with band-pass fixed at 16 nm. Phosphorescence, lifetimes, and ODMR were obtained using this excitation setup. Phosphorescence decays were signal-averaged and analyzed by computer using a nonlinear least-squares Marquardt algorithm designed to minimize the χ^2 of the fitting function and whose goodness-of-fit was monitored with a residuals plot. Values of Φ_p/Φ_f were obtained by integrating the areas of fluorescence and phosphorescence spectra and corrected against a 1 mg/mL solution of L-tryptophan in 1:1 (v/v) ethylene glycol/water for which $\Phi_p/\Phi_f = 0.28$ (Longworth, 1971; Miller & King, 1975). For experiments performed at temperatures above that of liquid nitrogen, the instrumentation used was essentially that reported by Zang and Maki (1990) with the important addition of a temperature controller (Lake Shore Cryotronics, Model 805). Temperatures were monitored in this apparatus with a silicone diode sensor (accuracy is within ±1% of the actual temperature).

For all measurements, the samples were placed in 1-mm Suprasil tubes which were then frozen in a Janis Research cryostat. Several methods of sample freezing were used. In some experiments, the sample was inserted directly into liquid helium so that the ~10-μL sample was frozen very rapidly. For other measurements, the sample was slowly placed in the Dewars' helium-gas-charged inner chamber which is cooled by a liquid nitrogen jacket to temperatures between 150 and 80 K so that the solution froze "slowly". Differences in phosphorescence and ODMR spectral characteristics could not be correlated with the preparation of the glassy matrices.

Table I: Triplet-State Properties of Trp29 in Snake Venom Neurotoxins

sample[a]	λ_{exc}[b] (nm)	$\lambda_{emission}$[c] (nm)	lifetimes[d] (s)
BgTX[e]	285	410.9–411.9	(35–55) 0.6–1.5, (45–65) 5.0–6.0
	300	411.3–412.3	
$BgTX_{red}$	285	410.1	(7) 3.5, (93) 7.0
	300	410.9	(6) 1.7, (94) 6.9
CbTX[e]	285	410.9–411.3	(21–44) 0.2–1.5, (57–78) 4.9–6.7
	300	411.3–411.7	
$CbTX_{red}$	285	409.9	(9) 3.1, (91) 7.0
	300	410.7	(7) 1.1, (93) 6.9
CoTX	285	411.1	(100) 6.6
	300	411.5	(100) 6.7

[a] All samples were in water and contained 30% ethylene glycol. [b] Wavelength of excitation. [c] The assigned 0,0-band of Trp29 at which all kinetic measurements were made. $\lambda_{emission}$ values for BgTX and CbTX are reported as ranges which reflect the variability observed for the phosphorescence 0,0-band in different samples. [d] Lifetimes were extracted from the observed decays at 4.2 or 77 K using a least-squares technique. The percentage of the total emission is presented in parentheses immediately preceding the extracted lifetime. [e] The ranges of lifetimes and their preexponential values reported for BgTX and CbTX are applicable for excitation both at 285 and at 300 nm.

RESULTS

Phosphorescence. The phosphorescence spectra of BgTX and CoTX are shown in Figure 1 using excitation centered at 285 and 300 nm. As is apparent, the phosphorescence of Trp29 in BgTX (Figure 1A) is not as well resolved as that observed from CoTX (Figure 1B). The band structure of Trp29 phosphorescence in CbTX is broader than that of BgTX. Using 300-nm excitation, the position of the 0,0-band maximum of BgTX changes over a considerable range of 411.3–412.3 nm from one frozen sample to another. This variation in the origin of phosphorescence emission was observed for CbTX as well, although the range of wavelengths is considerably less. We report the observed ranges of the phosphorescence 0,0-bands for the two differing excitation routines in Table I. The phosphorescence 0,0-bands of different frozen samples of CoTX did not vary in their position in the manner reported above for BgTX and CbTX. They are found at 411.1 and 411.5 nm for 285- and 300-nm excitation, respectively (see upper and lower spectra of Figure 1B, respectively). Excitation at the long-wavelength edge of the absorption band results in a bathochromic shift of 0.4 nm in the phosphorescence of BgTX, CbTX, and CoTX (Table I). Although this shift is only slightly larger than experimental uncertainty, it is highly reproducible as well as independent of the shifts in the phosphorescence 0,0-band observed for different frozen samples of BgTX and CbTX reported above. The phosphorescence wavelengths of Trp residues exposed to polar solvents typically exhibit a larger dependence on the wavelength of excitation than do buried Trp residues. For comparison, under identical conditions in our spectrophotometer, the phosphorescence of L-tryptophan in frozen aqueous solution exhibits a bathochromic shift of 1.5 nm upon an excitation change from 285 to 300 nm, in good agreement with previous observations (Galley & Purkey, 1970; Hershberger et al., 1980), while the hormone somatostatin exhibits a 1.2-nm bathochromic displacement of its single solvent-exposed Trp residue. No tyrosine phosphorescence is observed to shorter wavelengths of the Trp phosphorescence irrespective of the exciting wavelength. This indicates that Tyr25, present in all three neurotoxins, and additionally Tyr55 of BgTX and Tyr39 of CoTX are internally quenched, in common with many

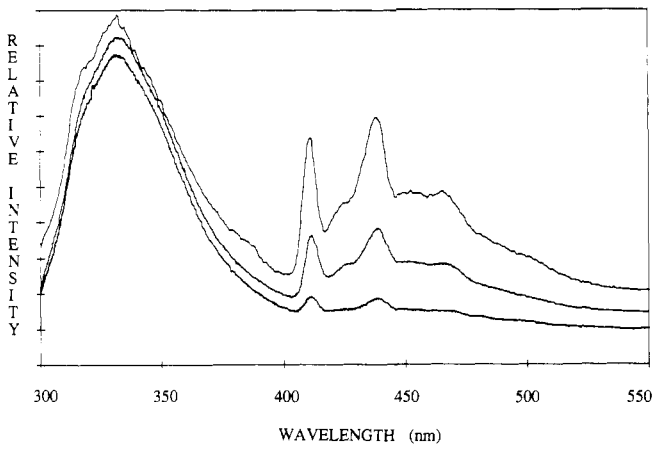

FIGURE 2: Total luminescence spectra of, from top to bottom, CoTX, $BgTX_{red}$, and BgTX. Spectra were recorded at 77 K with excitation centered at 295 nm and ~8-nm band-pass.

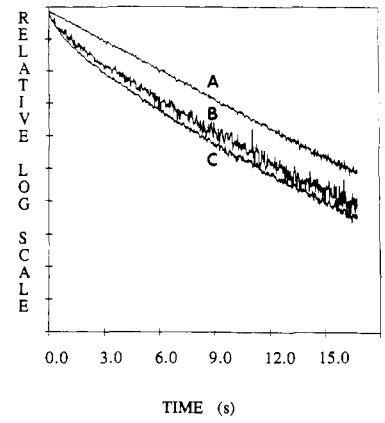

FIGURE 3: Natural log of the phosphorescence decay of Trp29 shown for (A) CoTX and (B and C) BgTX. For (A) and (C), λ_{exc} = 300 nm, and in (B), λ_{exc} = 285 nm. All three responses were observed at 4.2 K while observing the apex of the phosphorescence 0,0-band of tryptophan following excitation for a period of 30.0 s.

proteins that contain both Tyr and Trp (Longworth, 1971). Qualitatively, the phosphorescence of BgTX and CbTX is much weaker than that of CoTX. Upon reduction of Cys30–Cys34 in BgTX and CbTX, an increase in emission intensity is observed. The phosphorescence spectra of $BgTX_{red}$ and $CbTX_{red}$ were found to be better resolved and also blue-shifted with respect to those observed in BgTX and CbTX, respectively. Furthermore, upon changing the excitation wavelength from 285 to 300 nm, a 0.8-nm bathochromic shift is observed for both $BgTX_{red}$ and $CbTX_{red}$ (Table I).

Total Luminescence. The triplet state of Trp29 in BgTX is quenched selectively as suggested by the total luminescence spectra which are compared in Figure 2. For BgTX, the ratio of Φ_p/Φ_f was determined to be 0.02 both at 77 K and at at 4.2 K. The selective reduction of the disulfide between Cys30–Cys34 results in an increase in Φ_p/Φ_f of Trp29 to 0.10, suggesting the involvement of this cystine bridge in the triplet-state deactivation. This interpretation is consistent with our measured values of Φ_p/Φ_f = 0.21 for the homologous short-chain toxin CoTX in which the fifth disulfide is absent. The ratio of phosphorescence to fluorescence intensity for $BgTX_{red}$, although 5-fold larger than that of BgTX, is only half the value found for CoTX. This suggests that stoichiometric reduction of Cys30–Cys34 may not have been achieved in our procedure. The triplet-state kinetics presented below give additional evidence for the involvement of the Cys30–Cys34 disulfide in the quenching of Trp29 in BgTX.

Triplet-State Kinetics. In contrast with tryptophan fluorescence which exhibits nonexponential behavior in most cases (Beechem & Brand, 1985; Alcala et al., 1987), tryptophan phosphorescence decays, with only rare exceptions, as a single exponential at temperatures sufficiently high that spin–lattice relaxation dominates over the $T_1 \rightarrow S_0$ decay rates (Longworth, 1971). The triplet-state emission of Trp29 in both BgTX and CbTX is decidely nonexponential at 77 K and at 4.2 K (Figure 3). Furthermore, the decay kinetics observed for these two proteins following continuous optical pumping for 30 s varied from sample to sample. This complex behavior reflects the variability observed in the phosphorescence emission origins reported above for BgTX and CbTX. The observed lifetimes and the range of their fractional contributions to the total emission are reported in Table I. They represent the range spanned by many independent measurements which were modeled as biexponentials. Optically pumping BgTX at 300 nm (Figure 3C) leads to decays which are on the average faster than those observed with 285-nm excitation (Figure 3B). A similar dependence of observed lifetimes on excitation wavelength, shorter overall lifetimes for longer-wavelength excitation, is observed as well for CbTX. Even though there was slight variation in the observed lifetimes of BgTX and CbTX with each frozen sample, it is important to note that there was no appreciable difference between observations made at 77 K and those made at 4.2 K using the same frozen sample. Indeed, the decay profile observed for one sample of BgTX frozen at 80 K was found to be invariant up to 150 K. No changes were discernible in the phosphorescence kinetics of CbTX frozen at 4.2 K until temperatures were above 160 K. These results are consistent with the lack of temperature dependence of Φ_p/Φ_f reported above for BgTX. The emission of Trp29 in CoTX is typical of an unperturbed Trp residue with a single-component lifetime of 6.7 s. Both $BgTX_{red}$ and $CbTX_{red}$ exhibit nearly monoexponential decays with the major lifetime component very close to that observed for CoTX, as presented in Table I. The presence of a minor second, shorter lifetime component in these samples suggests the incomplete cleavage of Cys30–Cys34. These observations of phosphorescence decay kinetics and the previously discussed dependence of Φ_p/Φ_f upon the redox state of Cys30 and Cys34 clearly establish that the triplet state of Trp29 is perturbed by the neighboring disulfide.

ODMR. In Figure 4A (top spectrum), we present the slow-passage ODMR of BgTX, obtained using 285-nm excitation, which is typical of Trp ODMR in that both the D–E resonance at ~1.8 GHz and the 2E signal at ~2.6 GHz are observed as increases in phosphorescence intensity, $\delta P > 0$, and the D+E signal at ~4.2 GHz is absent. When the excitation monochromator is changed to a band centered at 300 nm, the bottom spectrum of Figure 4A is observed. Most noticeable is the change in polarity, $\delta P < 0$, of the signal in the Trp D–E region. This signal originates from Trp29; Tyr, the only other amino acid in which ODMR may be observed, has resonances at 2.20 and 5.59 GHz (Zuclich et al., 1973). Using excitation which is intermediate in wavelength to the above or using a broader excitation bandwidth results in the disappearance of the D–E signal into the base line. This is the first report of a negative Trp ODMR D–E signal for a free protein. Also in evidence is a weak negative polarity D+E signal observed when using 300-nm excitation. As shown in Figure 4A, the D–E signal obtained with higher excitation wavelength appears to be shifted to lower frequencies. ODMR line positions, however, depend on the scan rate of the microwave frequency and upon the triplet-state sublevel dynamics. When corrections for these "rapid passage effects"

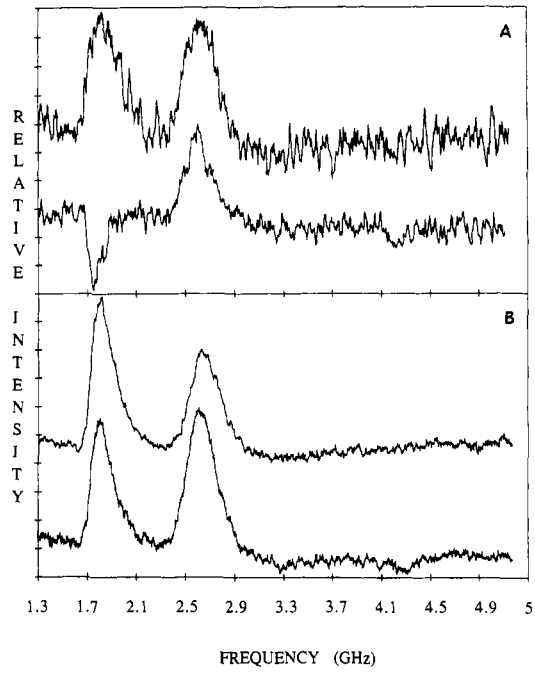

FIGURE 4: ODMR spectra of (A) BgTX and of (B) $BgTX_{red}$ observed at 1.2 K. Within each panel, the top spectrum was obtained with excitation centered at 285 nm with 16-nm band-pass and the bottom spectrum with excitation centered at 300 nm with 16-nm band-pass. All spectra were recorded at a microwave sweep rate of 64 MHz s^{-1} while observing the apex of the phosphorescence 0,0-band of tryptophan.

Table II: Slow-Passage ODMR Transitions of Trp29 in Snake Venom Neurotoxins

sample[a]	λ_{exc}[b] (nm)	$\lambda_{emission}$[c] (nm)	D–E[d] (GHz)	2E[d] (GHz)	D+E[d] (GHz)
BgTX	285	411.8	(+) 1.69	(+) 2.53	
	300	412.2	(–) 1.68	(+) 2.51	(–) 4.16
$BgTX_{red}$	300	410.9	(+) 1.74	(+) 2.56	(–) weak
CbTX	285	411.3	(+) 1.68	(+) 2.51	
	300	411.7	(–) 1.69	(+) 2.49	(–) 4.20
$CbTX_{red}$	300	410.7	(+) 1.61	(+) 2.43	(–) weak
CoTX	285	411.1	(+) 1.70	(+) 2.55	
	300	411.5	(+) 1.70	(+) 2.54	

[a] All samples were in water and contained 30% ethylene glycol. [b] The wavelength of excitation. [c] The emission wavelength of Trp29 at which ODMR measurements were made. [d] The parentheses preceding the ODMR frequencies indicate whether the observed transition is an increase (+) or decrease (–) in phosphorescence intensity with respect to the total steady-state emission. D–E and 2E transitions are corrected for rapid-passage effects, but the D+E transition is not.

in the slow-passage experiments are made (Ross et al., 1977; Khamis et al., 1987), the true ODMR frequencies observed using the two excitation routines are identical within experimental uncertainty (Table II). The apparent displacement of the D–E signal observed with 300-nm excitation and a scan rate of 64 MHz s^{-1} to lower frequencies than the D–E signal observed with 285-nm excitation and an identical scan rate suggests that with 300-nm excitation we are probing a subensemble of the total Trp population which is characterized by faster sublevel dynamics. We suggest that this environment is one in which Trp29 moves closer to the sulfur residues of the Cys30–Cys34 disulfide. This interpretation is consistent with the observation of faster triplet-state deactivation when using 300-nm excitation as compared with 285-nm excitation, given that this disulfide has been established above as a Trp triplet-state quencher and that the Trp–disulfide quenching mechanism is distance-dependent (Li et al., 1989). The ODMR spectra of CbTX, measured under identical conditions

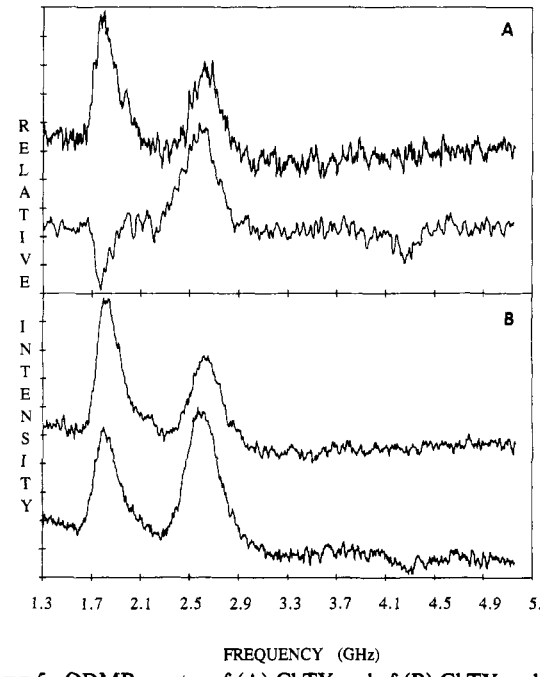

FIGURE 5: ODMR spectra of (A) CbTX and of (B) $CbTX_{red}$ observed at 1.2 K. Within each panel, the top spectrum was obtained with excitation centered at 285 nm with 16-nm band-pass and the bottom spectrum with excitation centered at 300 nm with 16-nm band-pass. Each spectrum was recorded at a microwave sweep rate of 64 MHz s^{-1} while observing the apex of the phosphorescence 0,0-band of tryptophan.

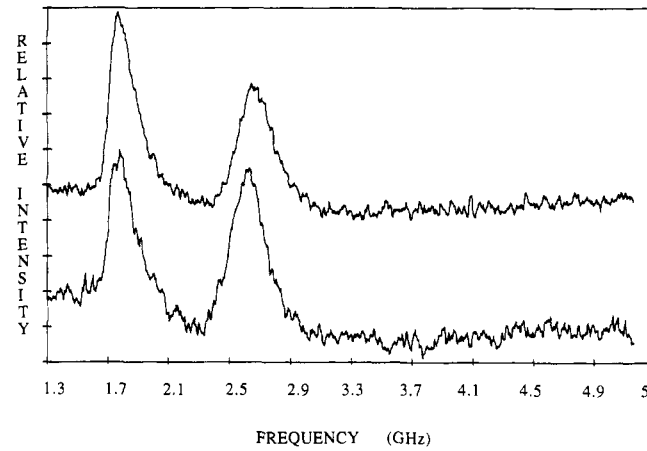

FIGURE 6: ODMR spectra of CoTX observed at 1.2 K. The top spectrum was obtained with excitation centered at 285 nm with 16-nm band-pass and the bottom spectrum with excitation centered at 300 nm with 16-nm band-pass. Each spectrum was recorded at a microwave sweep rate of 64 MHz s^{-1} while observing the apex of the phosphorescence 0,0-band of tryptophan.

as those used for BgTX, are displayed in Figure 5A, and the results are tabulated in Table II. The similarity in the spectral dependence on excitation conditions to that found in BgTX is striking. As in BgTX, broad-band excitation decreases the D–E signal to base line [this absence of the D–E signal of CbTX using broad-band excitation has been reported also by Tringali et al. (1991)]. The highly unusual and remarkably similar set of ODMR signals observed for Trp29 in both BgTX and CbTX suggests a very similar distribution of environments. That the ODMR spectra of Trp29 in BgTX and CbTX reflect the presence of Cys30–Cys34 is verified by observations made on $BgTX_{red}$ (Figure 4B) and $CbTX_{red}$ (Figure 5B). Both D–E and 2E transitions are "normal" in the sense that their polarity with respect to the total emission is positive, and independent of excitation wavelength. The presence of a weak, negative polarity, D+E signal upon excitation at 300 nm, barely visible

in the lower spectra of Figures 4B and 5B, suggests that some bridges between Cys30 and Cys34 are still intact as has been suggested above. For comparison, in Figure 6 we present the ODMR spectra of the Trp29 of CoTX, which lacks the fifth cystine, using the two different excitation conditions.

It is apparent from Figure 6 and also from Figures 4B and 5B that excitation at 285 nm increases the ratio of the intensity of the D–E slow-passage signal to that of the 2E resonance, I^{D-E}/I^{2E}, relative to that observed using excitation at 300 nm. We have observed similar excitation dependence of I^{D-E}/I^{2E} in frozen aqueous solutions of L-tryptophan, 3-methylindole, and HEWL (data not presented). Several effects may contribute to this apparently general observation. We have presented evidence above suggesting the presence of residual amounts of disulfide-perturbed Trp29 in $BgTX_{red}$ and $CbTX_{red}$. Any contribution of a D–E signal of negative polarity, $\delta P < 0$, which is shown above to be enhanced via 300-nm excitation, will result in a decrease of $(I^{D-E}/I^{2E})_{300nm}$ relative to $(I^{D-E}/I^{2E})_{285nm}$. Thus, the excitation dependence of I^{D-E}/I^{2E} presented for $BgTX_{red}$ and $CbTX_{red}$ may reflect, in part, the contribution of disulfide-perturbed Trp. A more general explanation for the phenomenon arises from a consideration of terms higher than first order in optical pumping rate in the derivation of the ODMR slow-passage equation (eq 1, presented below) (Maki, 1984). In our apparatus, the excitation intensity is about a factor of 5 greater at 300 nm than at 285 nm. This experimental increase in available intensity at the longer wavelength is more than offset by a greater than 5-fold decrease in the extinction of Trp at 300 nm versus 285 nm. The fact that the excitation wavelength dependence of I^{D-E}/I^{2E} depends upon beam intensity is experimentally verified by observations on L-tryptophan in an ethylene glycol/water glass and on CoTX in which $(I^{D-E}/I^{2E})_{300nm}$ can be made to equal $(I^{D-E}/I^{2E})_{285nm}$ by suitable attenuation of the excitation beam with neutral density filters. It must be emphasized that the ODMR signals for BgTX and CbTX with excitation centered at 300 nm retain their characteristic signal polarities, $\delta P < 0$ for the D–E and $\delta P > 0$ for the 2E resonances, when the optical pumping intensity is attenuated and therefore are not the result of an experimental artifact.

Unfortunately we are not able to extract sublevel dynamics for the disulfide-perturbed Trp29 of BgTX or CbTX due to their complex decay behavior.

Discussion

We have shown above that the triplet state of Trp29 in BgTX and CbTX is quenched and have identified the responsible agent as the proximal disulfide, Cys30–Cys34. Although the results are complex, it was demonstrated that there is enhancement of the disulfide-perturbed Trps upon excitation into the red-edge of the absorption band. In the following discussion, we wish to focus on three areas. First, we will address the range of values reported for different frozen samples of BgTX and CbTX. Of particular relevance in this discussion is how our spectroscopic results, obtained in frozen glasses, may be reconciled or compared with the previous structural determinations in fluid solution and in the crystalline state. Second, we will consider the excitation dependence of Trp triplet-state properties observed here for all samples. Our goal, in this section, is to better characterize the position of Trps within the toxin with respect to the protein and solvent. Lastly, we will discuss the mechanism of Trp–disulfide interactions.

Toxin Flexibility in the Trp29 Region. The phosphorescence origins of different frozen samples of BgTX and CbTX are observed to vary over the range 410–412 nm. This variation is also reflected in small changes of the lifetimes observed in these samples. Such variability in spectral properties must reflect differences in the disposition of Trp29 in the protein–solvent matrix into which it is entrapped at low temperatures prior to spectroscopic measurements. First, let us consider whether or not the addition of cryosolvent to our samples causes an undue structural perturbation. It is well-known that the addition of polyhydroxylic substances to aqueous solutions stabilizes protein conformation (Gekko & Timasheff, 1981). The stabilizing effect occurs through preferential exclusion of polyols from the protein–solution interface, or conversely stated, preferential protein hydration occurs (Gekko & Timasheff, 1981; Arakawa & Timasheff, 1985). Unless the enzyme specifically binds the cryosolvent and therefore induces changes in the tryptophan environment, as is the case for ethylene glycol binding in the active site of HEWL (Ikeda & Hamaguchi, 1970), the cryosolvent in concentrations up to 50% (Tanford, 1968) is rather benign. The mechanism of preferential protein hydration has also been invoked to explain the cryoprotective properties of polyols upon freezing of protein samples (Carpenter & Crowe, 1988; Carpenter et al., 1989). Therefore, in rapidly frozen cryosolvent-containing protein solutions, it is water that is in intimate contact with the protein, and the protein is in solution-like conformational states. Thus, we believe that the addition of the cryosolvent, ethylene glycol, to the sample solution in the concentrations used here, 30%, does not significantly alter the microenvironment of Trp29 in the neurotoxin proteins studied.

There is good evidence to suggest that the toxin reactive surface containing Trp29 is flexible. Temperature-dependent NMR and CD experiments on BgTX (Inagaki et al., 1985) and CbTX (Hilder et al., 1982) over the range of 20–70 °C clearly establish a change in the environment of Trp29. The absence of temperature-dependent shifts in the region of the CD spectra assigned to the amide backbone over this temperature range indicates that the change in conformational states of Trp29 does not involve the flipping of Trp29 to the opposite side of the molecule (Inagaki et al., 1985). Such conformations, with Trp29 positioned on the convexed side of the reactive surface, as found in the crystal structure of BgTX, apparently are induced by packing interactions (Love & Stroud, 1986; Basus et al., 1988). The existence of different protein conformers in room temperature solutions also is suggested by the multiplicity of fluorescence lifetimes, some of which are unusually short, observed for BgTX and CbTX (Pearce & Hawrot, 1991).

We envision that the variability in spectral properties observed in the long-chain toxins in frozen media reflects the populations of multiple conformers in the solution phase. Upon lowering the temperature, there will be a redistribution of populations among these conformational states, the kinetics of which depend critically on several factors such as protein flexibility, solvent composition, and the rate of temperature change. Thus, the possibility exists to entrap several almost equipotential conformers in low-temperature glasses. In some of these conformations, the distance and orientation of Trp29 relative to Cys30–Cys34 will vary subtly, and given the extreme sensitivity of the Trp–disulfide interaction to their separation (see below), this will lead to variations in observed lifetimes. Variability in phosphorescence spectral shifts among different frozen samples may arise through a similar mechanism involving differing population distributions between the many conformer states.

It is interesting that we do not observe a range of spectral properties for different frozen samples of CoTX as we do for

BgTX and CbTX. On the basis of a comparison of rates of deuterium exchange of the β-pleat amide protons between long- and short-chain toxins, the order of structural rigidity was inferred to be long-chain > short-chain (Endo et al., 1981). It is reasonable to expect that the greater the structural rigidity of a toxin, the smaller will be the range of entrapped conformations that form upon freezing. The spectral variability we report here for different frozen samples of BgTX and CbTX therefore must reflect, in large part, the special role of the neighboring disulfide (absent in CoTX) as a reporter of local structural disorder.

Excitation Dependence. Often the position of the phosphorescence spectrum in rigid media is used to classify whether or not a Trp residue is buried or exposed. As pointed out by Strambini and Gabellieri (1989), Trp phosphorescence in nonpolar solvents peaks in the 412–413-nm region, and any shift to the red of these wavelengths can be safely attributed to a residue buried in a hydrophobic environment. For emission occurring to the blue of 412–413 nm, the situation is not so straightforward. A residue may be buried or partially buried but still be in the neighborhood of a polar residue. The effect of the local charge is to destabilize the triplet state of Trp and shift the emission to shorter wavelengths (Galley & Purkey, 1970). An excellent example of the latter case is the single Trp of RNase T1. Its highly resolved Trp phosphorescence reflects its positioning within the ordered protein interior, yet its emission peaks at 404.5 nm (Hershberger et al., 1980), a wavelength shorter than that observed for Trp in aqueous glasses, 407 nm (Galley & Purkey, 1970; Hershberger et al., 1980). In light of the above considerations, it is difficult to classify the observed emission of Trp29 in the neurotoxins investigated here as characteristic of either a buried or an exposed residue. Previous studies on neurotoxins using a variety of techniques suggest that Trp29 is either buried or partially buried (Chicheporte et al., 1972; Menez et al., 1976a,b) or exposed (Seto et al., 1970; Muszkat et al., 1984). Crystallographic studies show that the single Trp of erabutoxin b is half-buried in a hydrophobic cleft, making 17 van der Waals packing interactions with the 2 Ile residues between which it is sandwiched (Low & Corfield, 1986).

Perhaps a better indicator of the local environment of a Trp residue, whether it is buried or exposed, is the dependence of phosphorescence on the wavelength of excitation. Polar aromatic chromophores fixed in rigid polar solvents invariably yield red-shifted phosphorescence when excited to the red edge of their absorption bands. This general phenomenon has been reported by many groups, and the results have been interpreted as evidence of several distinct solute–solvent sites of varying electronic energy (Galley & Purkey, 1970; Itoh & Azumi, 1973, 1975). The magnitude of the excitation-dependent emission shifts observed for BgTX, CbTX, and CoTX, 0.4 nm for the two excitation routines used here, is significantly smaller than the 1.5-nm shift found for Trp exposed to the full spectrum of solvent interactions or for the 1.2-nm shift found for the solvent-exposed Trp of the small peptide somatosatin. This criterion leads to the conclusion that Trp29 is not solvent-exposed in any of the "native" neurotoxins. This is consistent with a recent NMR structural determination of BgTX which places Val40 directly in front of the Trp29 ring (Basus et al., 1988). For both $BgTX_{red}$ and $CbTX_{red}$, we observed a larger bathochromic shift of 0.8 nm upon changing the excitation wavelength from 285 to 300 nm. This observation suggests that disruption of the fifth disulfide of the long-chain toxins may increase solvent accessibility to Trp29. This interpretation is consistent also with $BgTX_{red}$ and $CbTX_{red}$ having the most blue-shifted phosphorescence origins of the neurotoxins studied here.

Trp–Disulfide Quenching. The phosphorescence study of Trp–disulfide quenching is problematic in that the triplet state is commonly populated through excitation via the singlet state. Disulfides are efficient quenchers of Trp fluorescence, resulting in decreased triplet-state populations. The dominant process involved in singlet-state aromatic deactivation in the presence of disulfides appears to arise from ground-state complexation (Sanyal et al., 1989; Swadesh et al., 1987). However, collisional quenching (Sanyal et al., 1989; Cowgill, 1970) or long-range energy transfer (Szmacinski et al., 1991), via a Förster mechanism (Förster, 1959), cannot be ruled out. In this work, we have demonstrated that Trp29 in BgTX and CbTX is quenched in the triplet state by the neighboring disulfide. It is not surprising, therefore, to find that Trp29 fluorescence also is quenched. Measurements of anomalously shortened singlet-state lifetimes (Pearce & Hawrot, 1991), reduced quantum yield (Pearce & Hawrot, 1990) for BgTX, and an order of magnitude larger fluorescence intensity of Trp29 at pH 7 in CoTX compared with BgTX [see Figure 5 in Chang et al. (1990)] suggest the presence of Trp–disulfide interactions leading to quenching of the singlet state at room temperature.

Recently, Li et al. (1989) have studied the action of two disulfide quenchers on the triplet state of an indole derivative in a glassy matrix at 77 K. The quenching of the phosphorescence by disulfide was shown to follow a Dexter-like (Dexter, 1953) exponential dependence, $k_q = K \exp(-2x/L)$, where $K = 2.2 \times 10^4$ s^{-1} is the limiting quenching rate constant at van der Waals contact (taken to be 4 Å), x is the separation beyond van der Waals contact, and $L = 0.75$ Å is the average effective Bohr radius for interaction. The small value of L implies that the interaction is highly localized; thus, a 10–20-fold reduction of the quenching rate constant is predicted for a change in separation of indole and disulfide of ~1 Å. On the basis of the observation that the anomalously shortened Trp phosphorescence of HEWL observed at 77 K becomes monoexponential at 4.2 K (von Schütz et al., 1974), Li et al. (1989) argue that the quenching process may arise from thermally activated energy transfer from the triplet state of Trp(s) to a disulfide. Clearly, our identification of a contiguous disulfide as the triplet-state quenching agent in the long-chain toxins coupled with its lack of temperature dependence over the range of from 4.2 to ~150 K is not consistent with such a mechanism. We believe that other processes may be operative in the much more complex HEWL system and that the single Trp-containing toxins studied here better model the quenching process of neighboring disulfides. HEWL contains six Trp residues and multiple Trp–disulfide encounters. The existence of triplet–triplet energy transfer among these Trp residues has been suggested previously (Longworth et al., 1976; Rousslang et al., 1976; Li & Galley, 1989). That energy-transfer processes from one or more Trps to other Trp(s) are occurring in HEWL is consistent with our observation of a ~100-cm^{-1} hypochromic shift of Trp phosphorescence upon cooling of HEWL from 77 to 4.2 K (data not presented). Thus, the anomalous temperature dependence of triplet-state deactivation observed in HEWL appears to be due to intraprotein energy transfer among multiple chromophores, some of which are perturbed by disulfide, and should not be interpreted as characteristic of primitive chromophore–disulfide interactions. Whatever the nature of the processes occurring in the HEWL system, the lack of known disulfide acceptor states of energy lower than that of the Trp triplet state, coupled

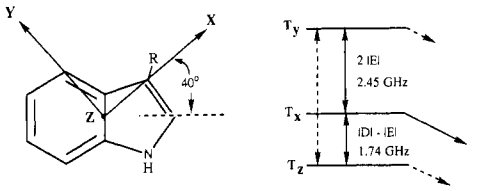

	k_i (s^{-1})	k_i^r	N_i^0
T_y	0.119	<0.1	0.97
T_x	0.240	1.0	0.78
T_z	0.038	<0.1	1.0

FIGURE 7: Relationship of the molecular framework of tryptophan to the principal axes system. Also shown is the energetic disposition among the triplet-state sublevels. A dashed arrow indicates deactivation that is primarily radiationless while a solid arrow implies that radiative processes are primarily involved. Values for the total rate constants and relative values for the radiative rate constants and steady-state populations are presented below the energy diagram (Zuclich et al., 1973, 1974).

with the observation of a disulfide-induced quenching process at 4.2 K, suggests we are probably observing an electron-transfer process from Trp29 to Cys30–Cys34 in the long-chain neurotoxins. This mechanism is well established for Trp quenching in solution. One-electron transfer from the triplet state of Trp to added disulfide in aqueous solution at room temperature has been shown to occur using triplet–triplet absorption techniques (Bent & Hayon, 1974). More recently, quenching of room temperature Trp phosphorescence in proteins by addition of several small quenching agents has been suggested to proceed via electron transfer (Vanderkooi et al., 1990; Mersol et al., 1991; Calhoun et al., 1988). The observation that the disulfide-induced perturbation of Trp29 is unchanged over such a large temperature range, from ~150 to 4.2 K, is surprising but not unusual given the well-established temperature independence of electron transfer for various photosynthetic proteins. The classic example is *Chromatium vinosum*, which exhibits temperature-independent electron transfer below 120 K (DeVault & Chance, 1966).

Although we are not able to obtain directly the sublevel-specific dynamics for disulfide-perturbed Trp29, we are able to make some inferences about these processes by comparing the perturbed Trp29 ODMR spectra with the known, unperturbed, Trp dynamics. As shown in Figure 7, the sublevel steady-state populations and the relative radiative rate constants are in the order $N_z \geq N_y > N_x$ and $k_x^r \gg k_y^r, k_z^r$, respectively. T_x is by far the most radiative sublevel, and its relative quantum efficiency, Q_x, is close to unity (Maki & Zuclich, 1975). Furthermore, it has been established for the weakly emitting sublevels T_z and T_y that $k_y^r > k_z^r$ and that the typical absence of the D+E signal may be attributed to similar steady-state populations, and the similarity of the relative sublevel quantum yields, i.e. $Q_y \sim Q_z$ (Weers & Maki, 1986). Use of this information and eq 1, which describes the

$$\delta P^{ij} \sim (N_j^0 - N_i^0)(Q_i - Q_j) \quad (1)$$

steady-state ODMR signal intensity for the $T_i \leftrightarrow T_j$ transition, correctly predicts that δP^{xy} and $\delta P^{xz} > 0$ and that $\delta P^{zy} \sim 0$ for unperturbed Trp. In the following analysis of disulfide-perturbed Trp29 observed with 300-nm excitation, we make the assumption that the presence of a neighboring disulfide does not induce an external heavy-atom effect (HAE). It is generally believed that HAEs have a larger influence on radiative properties of the triplet-state deactivation then on nonradiative decay (McGlynn et al., 1969). Thus, a HAE generally increases Φ_p/Φ_f (McGlynn et al., 1969). Indeed, if we assume that the toxin structure is not greatly altered in our DDT-reduced samples, our results indicate that it is the disulfide bond and not the "heavy-atom" sulfur that is the source of the Trp29 perturbation. We know of no reports in the literature ascribing an external HAE to cysteinyl residues. Therefore, for the perturbed Trp we suggest that the k_i^r values are unaffected, i.e., only k_x^r is appreciably radiative, and that only nonradiative rates out of the triplet manifold are influenced. Under this assumption, the observation of $\delta P > 0$ for the 2E resonance suggests that $N_y > N_x$ since $Q_x \geq Q_y$. A $\delta P < 0$ for the D-E transition requires that $N_x > N_z$ since $Q_x > Q_z$. For the normally unobserved D+E transition, the population ordering $N_y > N_x > N_z$ established above and the appearance of an ODMR response $\delta P < 0$ demonstrate that $Q_y > Q_z$, which is in accord with previous measurements (Weers & Maki, 1986).

We may interpret the ordering of the relative sublevel steady-state populations and sublevel quantum yields of the perturbed Trp29 in two ways. It is possible that a non-sublevel-selective process is occurring. If k_q is the nonspecific quenching rate constant, it can be shown that the fractional change in the steady-state sublevel population is given by $\delta N_i/N_i^0 = -k_q/(k_q + k_i)$, which is greatest for the sublevel with the smallest k_i. In the case of Trp, k_z is smallest; thus, N_z would be expected to undergo the largest disulfide-perturbed, non-spin-selective reduction of population in the steady state, in agreement with our experimental results. There also is the possibility that the quenching process is spin-sublevel-specific and favors the out-of-plane T_z sublevel. Such a selective quenching would be expected to decrease N_z and Q_z directly. It should be noted that triplet spin sublevel selectivity has been suggested by previous measurement of the electron-transfer quenching of the phosphorescence of Zn-substituted cytochrome *c* by a ruthenium(III) pentaammine complex attached to the protein (Zang & Maki, 1990). In this system, it was possible to obtain directly the triplet sublevel dynamics which suggested that the T_z sublevel which has its spin angular momentum aligned in the porphyrin plane exhibited enhanced quenching. Unfortunately, heterogeneity in the decay kinetics does not permit us to determine whether the disulfide-induced Trp29 phosphorescence quenching is spin sublevel specific or whether it affects all spin sublevels equally.

Registry No. BgTX, 11032-79-4; CbTX, 69344-74-7; CoTX, 12584-83-7; Trp, 73-22-3.

REFERENCES

Alcala, J. R., Gratton, E., & Prendergast, F. G. (1987) *Biophys. J. 51*, 925–936.

Arakawa, T., & Timasheff, S. N. (1985) *Biochemistry 24*, 6756–6762.

Basus, V. J., Billeter, M., Love, R. A., Stroud, R. M., & Kuntz, I. D. (1988) *Biochemistry 27*, 2763–2771.

Beechem, J. M., & Brand, L. (1985) *Annu. Rev. Biochem. 54*, 43–71.

Bent, D. V., & Hayon, E. (1974) *J. Am. Chem. Soc. 97*, 2612–2619.

Botes, D. P. (1974) *Biochim. Biophys. Acta 359*, 242–247.

Calhoun, D. B., Englander, S. W., Wright, W. W., & Vanderkooi, J. (1988) *Biochemistry 27*, 8466.

Carpenter, J. F., & Crowe, J. H. (1988) *Cryobiology 25*, 244–255.

Carpenter, J. F., Arakawa, T., Kita, Y. A., & Crowe, J. H. (1989) *Cryobiology 26*, 556.
Chang, C.-C., Kawata, Y., Sakiyama, F., & Hayashi, K. (1990) *Eur. J. Biochem. 193*, 567–572.
Chen, Y. H., Lo, T. B., & Yang, T. F. (1977) *Biochemistry 16*, 1826–1830.
Chicheportiche, R., Rochat, C., Sampieri, F., & Lazdunski, M. (1972) *Biochemistry 11*, 1681–1691.
Chicheporte, R., Vincent, J.-P., Kopeyan, C., Schweitz, H., & Lazdunski, M. (1975) *Biochemistry 14*, 2081–2091.
Corfield, P. W. R., Lee, T.-J., & Low, B. W. (1989) *J. Biol. Chem. 264*, 8714–8722.
Cowgill, R. W. (1970) *Biochim. Biophys. Acta 207*, 556–559.
DeVault, D., & Chance, B. (1966) *Biophys. J. 6*, 825–847.
Dexter, D. L. (1953) *J. Chem. Phys. 21*, 836–850.
Dufton, M. J., & Hilder, R. C. (1983) *CRC Crit. Rev. Biochem. 14*, 113–171.
Endo, T., Inagaki, F., Hayashi, K., & Miyazawa, T. (1981) *Eur. J. Biochem. 120*, 117–124.
Förster, Th. (1959) *Discuss. Faraday Soc. 27*, 7–17.
Galley, W. C., & Purkey, R. M. (1970) *Proc. Natl. Acad. Sci. U.S.A. 67*, 1116–1121.
Gekko, K., & Timasheff, S. N. (1981) *Biochemistry 20*, 4667–4676.
Ghosh, S., Petrin, M., & Maki, A. H. (1986) *Biophys. J. 49*, 753–760.
Hershberger, M. V., Maki, A. H., & Galley, W. C. (1980) *Biochemistry 19*, 2204–2209.
Hilder, R. C., Drake, A. F., Inagaki, F., Williams, R. J. P., Endo, T., & Miyazawa, T. (1982) *J. Mol. Biol. 158*, 275–291.
Ikeda, K., & Hamaguchi, K. (1970) *J. Biochem. (Tokyo) 68*, 785–791.
Inagaki, F., Hilder, R. C., Hodges, S. J., & Drake, A. F. (1985) *J. Mol. Biol. 183*, 575–590.
Itoh, K., & Azumi, T. (1973) *Chem. Phys. Lett. 22*, 395–399.
Itoh, K., & Azumi, T. (1975) *J. Chem. Phys. 62*, 3431–3438.
Kabat, E. A., & Meyer, M. M. (1961) in *Experimental Immunochemistry*, 2nd ed., p 22, Charles C. Thomas, Springfield, IL.
Karlsson, E. (1979) *Handb. Exp. Pharmacol. 52*, 159–212.
Khamis, M. L., Casas-Finet, J. R., & Maki, A. H. (1987) *J. Biol. Chem. 262*, 1725–1733.
King, L. A., & Miller, J. N. (1976) *Biochim. Biophys. Acta 446*, 206–213.
Li, Z., & Galley, W. C. (1989) *Biophys. J. 56*, 353–360.
Li, Z., Lee, W. E., & Galley, W. C. (1989) *Biophys. J. 56*, 361–367.
Longworth, J. W. (1971) in *Excited States of Proteins and Nucleic Acids* (Steiner, R. F., & Weinryb, I., Eds.) pp 319–484, Plenum Press, New York.
Longworth, J. W., McLaughlin, C. L., & Soloman, A. (1976) *Biochemistry 15*, 2953–2958.
Love, R. A., & Stroud, R. M. (1986) *Protein Eng. 1*, 37–46.
Low, B. W. (1979) *Handb. Exp. Pharmacol. 52*, 213–257.
Low, B. W., & Corfield, P. W. R. (1986) *Eur. J. Biochem. 161*, 579–587.
Low, B. W., & Corfield, P. W. R. (1987) *Asia Pac. J. Pharmacol. 2*, 115–127.
Maki, A. H. (1984) *Biol. Magn. Reson. 6*, 187–294.
Maki, A. H., & Zuclich, J. (1975) *Top. Curr. Chem. 54*, 115–163.
Martin, B. M., Chibber, B. A., & Maelicke, A. (1983) *J. Biol. Chem. 258*, 8714–8722.
McGlynn, S. P., Azumi, T., & Kinoshita, M. (1969) *Molecular Spectroscopy of the Triplet State*, Prentice-Hall, Englewood Cliffs, NJ.
Menez, A., Bouet, F., Fromageot, P., & Tamiya, N. (1976a) *Bull. Inst. Pasteur 74*, 57–64.
Menez, A., Bouet, F., Tamiya, N., & Fromageot, P. (1976b) *Biochim. Biophys. Acta 453*, 121–132.
Mersol, J. V., Steel, D. G., & Gafni, A. (1991) *Biochemistry 30*, 668–675.
Miller, J. N., & King, L. A. (1975) *Biochim. Biophys. Acta 393*, 435–445.
Muszkat, K. A., Khait, I., Hayashi, K., & Tamiya, N. (1984) *Biochemistry 23*, 4913–4920.
Pearce, S. F. A., & Hawrot, E. (1990) *Biochemistry 29*, 10649–10659.
Pearce, S. F. A., & Hawrot, E. (1991) *Biophys. J. 59*, 299a.
Reid, K. S. C., Lindley, P. F., & Thornton, J. M. (1985) *FEBS Lett. 190*, 209–213.
Ross, J. B. A., Rousslang, K. W., Deranleau, D. A., & Kwiram, A. L. (1977) *Biochemistry 16*, 5398–5402.
Rousslang, K. W., Thomasson, J. M., Ross, J. B. A., & Kwiram, A. L. (1979) *Biochemistry 18*, 2296–2300.
Sanyal, G., Kim, E., Thompson, F. M., & Brady, E. K. (1989) *Biochem. Biophys. Res. Commun. 165*, 772–781.
Seto, A., Sato, S., & Tamiya, N. (1970) *Biochim. Biophys. Acta 214*, 483–489.
Steiner, R. F., & Kirby, E. P. (1969) *J. Phys. Chem. 73*, 4130.
Strambini, G. B., & Gabellieri, E. (1989) *Biochemistry 28*, 160–166.
Swadesh, J. K., Mui, P. W., & Scheraga, H. A. (1987) *Biochemistry 26*, 5761–5769.
Szmacinski, H., Wiczk, W., Fishman, M. N., Eis, P. S., & Lakowicz, J. R. (1991) *Biophys. J. 59*, 116a.
Tanford, C. (1968) *Adv. Protein Chem. 23*, 121–282.
Tringali, A. E., Pearce, S. F. A., & Brenner, H. C. (1991) *Biophys. J. 59*, 301a.
Tsernoglou, D., & Petsko, G. A. (1976) *FEBS Lett. 68*, 14.
Vanderkooi, J., Englander, S. W., Papp, S., Wright, W. W., & Owen, C. S. (1990) *Proc. Natl. Acad. Sci. U.S.A. 87*, 5099–5103.
von Schütz, J. U., Zuclich, J., & Maki, A. H. (1974) *J. Am. Chem. Soc. 96*, 714–718.
Walkinshaw, M. D., Saenger, W., & Maelicke, A. (1980) *Proc. Natl. Acad. Sci. U.S.A 77*, 2400–2404.
Weers, J. G., & Maki, A. H. (1986) *Biochemistry 25*, 2897–2904.
Wilson, P. T., & Lentz, T. L. (1988) *Biochemistry 27*, 6667–6674.
Zang, L.-H., & Maki, A. H. (1990) *J. Am. Chem. Soc. 112*, 4346–4351.
Zuclich, J., Schweitzer, D., & Maki, A. H. (1973) *Photochem. Photobiol. 18*, 161.
Zuclich, J., von Schütz, J. U., & Maki, A. H. (1974) *Mol. Phys. 28*, 33–47.